

# Nuclear Physics Study of the Composition of Surface Layers of Rapidly Solidified Foils of Al–Mg–Li–Sc–Zr Alloy after Heat Treatment

I. A. Stoliar<sup>a, \*</sup>, V. G. Shepelevich<sup>a</sup>, I. I. Tashlykova-Bushkevich<sup>b, \*\*</sup>, and E. Wendler<sup>c</sup>

<sup>a</sup> Belarusian State University, Minsk, 220030 Belarus

<sup>b</sup> Belarusian State University of Informatics and Radioelectronics, Minsk, 220013 Belarus

<sup>c</sup> Friedrich-Schiller-Universität Jena, Jena, 07743 Germany

\*e-mail: uyluana@gmail.com

\*\*email: iya.itb@bsuir.by

Received June 26, 2022; revised July 22, 2022; accepted July 22, 2022

**Abstract**—The influence of heat treatment on the distribution of lithium over the depth of surface layers is studied for rapidly solidified foils of industrial Al–Mg–Li–Sc–Zr alloy (1421) produced by ultra-rapid quenching from the molten state using unilateral cooling on the internal surface of a rotating copper drum. It is found by electron backscatter diffraction that the as-cast foils had a micrograin structure with an average grain size of 12  $\mu\text{m}$  and the [111] texture. Using atomic-force microscopy, it is determined that the air-side surface is characterized by a fine cellular structure, which is also observed in the area of caverns and cavities on the drum-side surface. The surface roughness of the foils is from 44 to 57 nm. The patterns of the lithium depth distribution in the annealed samples are established by nuclear-reaction analysis using a proton-induced reaction ( $p, \alpha$ ). It is found that during low-temperature annealing, the surface and deep layers of the samples are depleted of lithium, which is evenly distributed over the foil depth. A multiple increase in the lithium concentration found in the surface region of the foils is established during high-temperature annealing, resulting in the formation of a composition-gradient foil structure. The effect of the structure and phase changes caused by the decomposition of a supersaturated solid solution with the precipitation of lithium-containing phases on the behavior of lithium in the annealing temperature range 150–380°C is discussed.

**Keywords:** rapid solidification, Al–Mg–Li–Zr–Sc alloy, lithium, electron backscatter diffraction, atomic-force microscopy, nuclear-reaction analysis

**DOI:** 10.1134/S1027451023010408

## INTRODUCTION

The main industrial consumers of aluminum-magnesium alloys are powder metallurgy, mechanical engineering, instrument making and enterprises that create aerospace equipment, for which it is important to improve the dynamic characteristics of products and reduce fuel consumption due to an increase in weight efficiency. Al–Mg binary alloys are the basis of nonthermal hardenable alloys of the 5XXX series according to the international classification [1] (according to the Russian classification, alloys of the AMg type). The addition of lithium to magnesium-containing aluminum alloys, which is the lightest metal, despite the complexity of the technology of melting products due to the chemical inhomogeneity of ingots, leads to a significant decrease in the density and increase in Young's modulus of the products. An increase in the level of mechanical properties of alloys, including strength, is achieved due to the precipitation

during heat treatment of strengthening metastable phases with lithium:  $\delta'$  ( $\text{Al}_3\text{Li}$ ) and  $S_1$  ( $\text{Al}_2\text{LiMg}$ ) [2, 3].

Since the current level of development of the aviation industry places increasing demands on the performance of industrial alloys based on the Al–Mg–Li system under conditions of elevated temperatures and humidity, it is advisable to use alloying with rare-earth- and transition metals to improve the set of unique properties that they possess. For example, among the advantages of multicomponent alloys of the Al–Mg system alloyed with scandium together with zirconium, which replaces part of the expensive scandium, high plasticity and thermal stability of dispersoids with high corrosion resistance, moderate strength, and good weldability are highlighted [4–6]. However, many of the alloying components of industrial aluminum alloys are poorly soluble in aluminum under equilibrium conditions. Therefore, in order to expand the range of products from magnesium-containing aluminum alloys, the search for resource-sav-

ing technologies for the synthesis of Al–Mg alloys of different alloying systems and optimal modes of hardening heat treatment [4, 7, 8] is being actively pursued, which will solve the problem of the negative influence of temperature effects on the physical, mechanical and chemical properties of the materials. In particular, the additional doping of magnesium-containing aluminum alloys with rare-earth- and transition metals is especially effective for high-speed crystallization [1, 9]. In rapidly solidified materials, structure modification [10] is provided by the formation of anomalously supersaturated solid solutions, the dispersion of structural components, and the formation of metastable intermediate phases.

The industrial use of rapidly solidified alloys requires a deep understanding of the structural-phase transformations that occur during heat treatment and their influence on the properties of alloys. Previously obtained experimental data [11, 12] point to the prospects for improving the properties of Al–Mg–Li-system alloys as a result of high-speed crystallization. Of particular interest is the revealed effect of the influence of the formation of a metastable Li-containing phases of variable composition  $\text{Al}(\text{Mg}, \text{Sc}, \text{Zr}, \text{Li})_x$  at temperatures around 300°C on the mechanical properties of rapidly solidified Al–Mg–Li–Sc–Zr (1421) industrial alloy foils, since this temperature satisfies the operating conditions at elevated temperatures and is close to the optimum temperature for obtaining solid products by compacting rapidly solidified samples. Therefore, of scientific and practical interest is a detailed study of the dependence of the microstructure and elemental composition of the surface layers of rapidly solidified Al–Mg–Li–Sc–Zr alloy on the annealing temperature to determine the structural-phase stability of the material. It is known that a significant effect on the properties of aluminum-based materials is provided by a protective oxide film, in the formation of which, in the case of 1421 alloy, lithium also participates. Its behavior has not been sufficiently studied in heat-treated multicomponent aluminum alloys. In particular, the depth profiling of lithium in aluminum alloys cannot be performed using traditional methods, such as X-ray microanalysis. Alternative methods used for measuring the microhardness or electrical resistance [13–15] also do not allow one to obtain unambiguous quantitative information about the lithium content in the surface layers and at a depth in alloys before and after annealing.

The aim of this work is a nuclear-physics study of the composition of the surface layers of rapidly solidified Al–Mg–Li–Sc–Zr-alloy foils after heat treatment. A comprehensive study of the structure of the surface of the samples is carried out using the methods of atomic-force microscopy (AFM), backscattered-electron diffraction, and the spectrometry of particle products of nuclear reactions. The use of AFM for microstructural studies, visualization and classification of the surface morphology of freshly quenched

samples, as well as the additional use of backscattered-electron diffraction, makes it possible to study their grain structure without preliminary preparation of foils. An important advantage of the nuclear-physics method of instantaneous nuclear reactions is that it can be used to solve the problem of detecting and quantitatively measuring the depth distribution profiles of foils of such a light element as lithium, depending on the heat-treatment conditions of the aluminum alloy. In addition, this method is nondestructive and is characterized by a high resolution and accuracy.

## EXPERIMENTAL

Foils of industrial aluminum alloy 1421 (Al 5.8 at %; Mg 8.1 at %; Li 0.03 at %; Zr 0.11 at %; Sc) were obtained by high-speed crystallization from the melt on the inner surface of a rotating copper cylinder 20 cm in diameter. The cylinder rotation rate was 1500 rpm and the cooling rate of the melt was about  $10^6$  K/s [16]. The thickness of the studied foils was 60–80  $\mu\text{m}$ . We considered side *A* as the contact surface of the foils adjacent to the copper cylinder and side *B* as the free surface of the foils in contact with air. Isothermal annealing of the foils was carried out at temperatures of 150, 220, 300 and 380°C, with holding for 1 h at each temperature.

The surface morphology of the freshly quenched foils was studied using an NT-206 atomic force microscope in the contact mode with the subsequent processing of  $20 \times 20 \mu\text{m}$  images using the SurfaceXplorer and SurfaceView programs (ODO Microtestmashiny, Belarus [17]). Backscattered-electron-diffraction patterns for analyzing the grain structure of foils were obtained using a scanning electron microscope LEO1455VP with an HKL CHANNEL5 attachment at an accelerating voltage of 20 kV using an EBSD detector. The scanning step was 2  $\mu\text{m}$ . Quantitative analysis of the grain structure was performed by the secant method using the OriginPro mathematical package.

To study the redistribution of lithium in the foils of the 1421 alloy during heat treatment, the method of instantaneous nuclear reactions was used using the nuclear reaction  ${}^7\text{Li}(p, \alpha){}^4\text{He}$  upon the irradiation of freshly quenched and annealed foils with accelerated protons with an energy of 1.4 MeV. The measurements were performed on a JULIA tandetron accelerator (3MV) (Jena University Laboratory for Ion Acceleration) with a detector resolution of 15 keV. The detector in the experiments was at an angle of  $\theta = 170^\circ$ . The diameter of the beam incident on the target was 1 mm. The resulting particle spectra were normalized to the height of the escape of backscattered protons on the left end of the spectrum, i.e., in the smallest channel of the low-energy region of the spectrum. Test experiments [18] carried out by the method of instantaneous nuclear reactions with a sample of lithium niobate ( $\text{LiNbO}_3$ ) containing 20 at % lithium, allowed use of

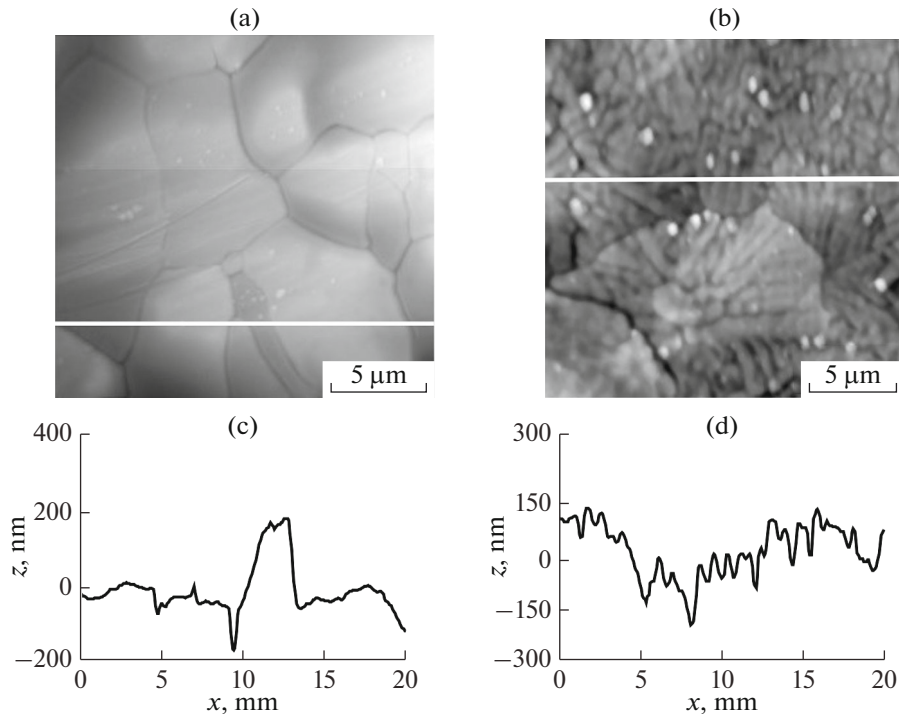


**Fig. 1.** AFM images of surfaces *A* (a) and *B* (b) of the freshly quenched foils of 1421 alloy and the corresponding diagrams of the distribution of asperities (c) and (d) along the scan lines highlighted in (a) and (b).

the SIMNRA computer program [19] for processing the spectra to determine the concentration of lithium in foils with an error of 11%. The methodology for processing the experimental spectra of backscattered protons and  $\alpha$  particles produced as a result of a nuclear reaction ( $p, \alpha$ ) was described earlier in [12]. The depth of analysis of the distribution of lithium over the thickness of the foils was 22  $\mu\text{m}$ .

## RESULTS AND DISCUSSION

Figures 1a and 1b show typical 2D topographic images of the surfaces of the freshly quenched 1421-alloy foils. The geometric characteristics of the roughness ensemble of both surfaces are similar. The height of peaks in individual areas of surface *A* can be 200 nm, and the depth of the depressions is 160 nm (Fig. 1c). On the opposite side, the maximum difference in the relief in certain areas of surface *B* reaches  $\sim 270$  nm (Fig. 1d). Both surfaces *A* and *B* are characterized by a cellular structure: on surface *A* cells are present in the region of depressions and air pockets, and on surface *B* over the entire surface area studied. The cell size on side *A* reaches 4  $\mu\text{m}$ , decreasing to 1  $\mu\text{m}$  on side *B*. Image distortions in the form of white dots (Fig. 1b) were taken into account as artifacts of the interaction of the probe with the surface and were excluded from analysis using standard algorithms that correct the influence of the probe geometry on the AFM images. The measured value of the roughness parameter  $R_a$  for

surfaces *A* and *B* of the foils is 56 and 44 nm, respectively.

An analysis of the backscattered-electron-diffraction patterns showed that, in the case of the used method of quenching on the cooling surface of a rotating cylinder, the resulting 1421-alloy foils are microcrystalline. They form a micrograin structure. Figure 2a shows a fragment of a high-resolution diffraction map of a typical surface area of a rapidly solidified 1421 alloy. In addition to areas with fine grains of average size up to 3  $\mu\text{m}$ , there are also areas with larger grains up to 20  $\mu\text{m}$  in size. Figure 2a additionally shows the color scale of orientations in the space of inverse pole figures for a face-centered cubic lattice. According to the obtained orientation maps, a texture is formed in the rapidly solidified foils of 1421 alloy [111].

Experimental data on the grain structure obtained by the method of backscattered-electron diffraction for surface *A* of the 1421-alloy foils (Fig. 2a) were approximated using the Gaussian distribution in the OriginPro mathematical package (Fig. 2b) with the coefficient of determination COD ( $R^2$ ), equal to 0.88 (Table 1). As can be seen from the figure, the size-group distribution of chords of random secants on grain sections can be described by a superposition of five Gaussian distributions. The positions ( $\ell_{\text{max}}$ ), height ( $f_{\text{max}}$ ), normalized area ( $S$ ), as well as the peak width at half maximum (FWHM) (Table 1). The average length  $\bar{\ell}$  of the chord of a grain of surface *A* is

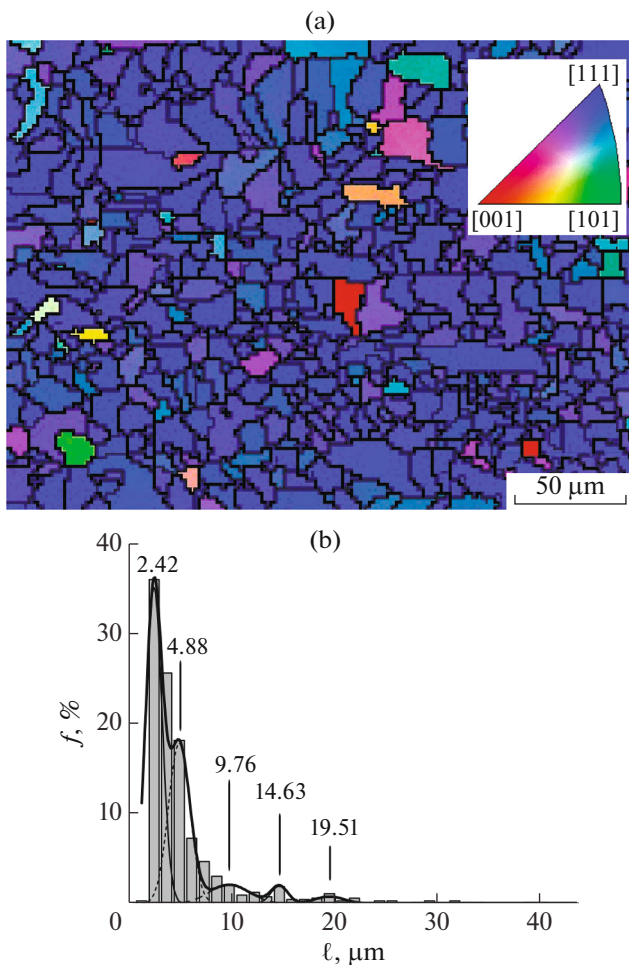


**Fig. 2.** Typical map of surface *A* of the freshly quenched foils of 1421 alloy, obtained by backscattered-electron diffraction (a) (color coding of crystallographic grain orientations in the inset), and the corresponding histogram of the chord size distribution of the grain cross sections of a given area of the foil surface (b).

equal to  $7.85 \mu\text{m}$ . If we take into account that the shape of the grains is polygonal (Fig. 2a), then, according to calculations by the well-known method [20], the average grain size of the foils is about  $12 \mu\text{m}$ .

As follows from Table. 1, the width and positions of the peaks in the distribution of chords of grain cross sections fluctuate in the case of fine and coarse grains. The amplitudes  $f_{\text{max}}$  of the peaks in the size distribution of the chords of sections of small grains up to  $5 \mu\text{m}$  in size are on average 17 times higher compared to the chords of the cross sections of large grains. In groups of smaller grains, the main portion of chords falls into size groups in the range from 1 to  $5 \mu\text{m}$ , and in the case of larger grains, from 7 to  $13 \mu\text{m}$ .

Experimental particle spectra (Figs. 3 and 4) were obtained for 1421-alloy foils freshly quenched and annealed by irradiation with accelerated protons. They represent the spectra of backscattered protons and  $\alpha$  particles produced as a result of the nuclear reaction ( $p, \alpha$ ). As can be seen from Fig. 3, in the left region of the experimental spectra, where backscattered protons are recorded, on the channel scale, the positions of well-distinguished signals of aluminum and lithium, as well as the accompanying elements of oxygen and carbon, localized near the foil surfaces, are marked by arrows. Since magnesium is an element adjacent in mass to aluminum, the signals of aluminum and magnesium in the spectra do not visually differ. It is also impossible to determine the signals of Sc and Zr alloying elements in the spectra of backscattered protons because of their low concentration in the 1421 alloy. In the right region of the spectra,  $\alpha$  particles from the reaction  ${}^7\text{Li}(p, \alpha){}^4\text{He}$  with lithium-7 are recorded, allowing its content in the samples to be studied.

The typical spectra of  $\alpha$  particles obtained from surfaces *A* and *B* of freshly quenched 1421-alloy foils (Fig. 3) are in good agreement with each other, indicating that there is no significant difference in the lithium concentration in the regions of both sides of the foils. In preliminary experiments [12], the depth profiles of lithium calculated from the spectra of the nuclear reaction  ${}^7\text{Li}(p, \alpha){}^4\text{He}$  using the SIMNRA program showed that the lithium signal is resolved to a depth of  $22 \mu\text{m}$ . Lithium is evenly distributed over the depth of the foils in the studied layers. Its measured concentration is 9.0 at % and differs from the calculated content in the alloy within the measurement

**Table 1.** Parameters of modeling approximating the histogram of the distribution of chords of grain sections by size groups on surface *A* of the 1421 alloy foils (Fig. 2a)

Secant method	OriginPro				
$\bar{\ell}, \mu\text{m}$	$\ell_{\text{max}}, \mu\text{m}$	$f_{\text{max}}, \%$	$S, \%$	FWHM	COD ( $R^2$ )
$7.85 \pm 0.79$	$2.42 \pm 0.80$	35.23	50.23	1.87	0.88
	$4.88 \pm 1.05$	17.91	36.08	2.47	
	$9.76 \pm 2.0$	2.14	8.14	4.65	
	$14.63 \pm 0.83$	1.99	3.16	1.94	
	$19.51 \pm 1.52$	0.82	2.39	3.57	

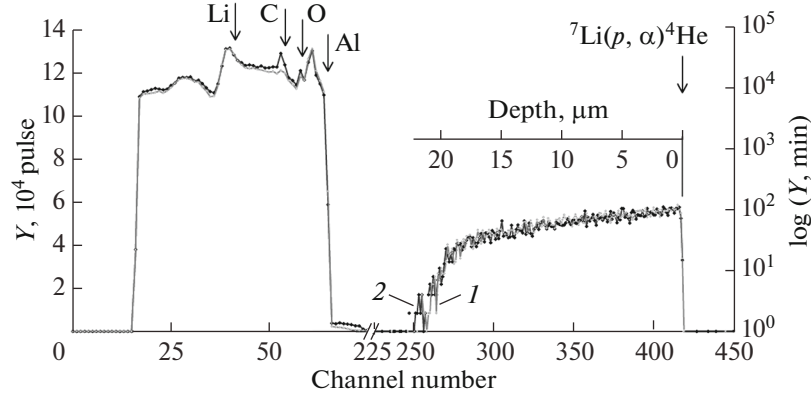


Fig. 3. Typical spectrum of scattered protons and products ( $p$ ,  $\alpha$ ) reactions for surfaces  $A$  (1) and  $B$  (2) of the freshly quenched 1421-alloy foils.

error by the method of instantaneous nuclear reactions.

It is known that determination of the composite composition of the samples is possible by comparing the integrated signals of the components in the spectra of scattered protons and products of ( $p$ ,  $\alpha$ ) reactions. This made it possible to construct (Fig. 5a) the temperature dependence of the normalized yield of lithium and oxygen particles in the spectra obtained by irradiating the annealed 1421-alloy foils with accelerated protons. The signals of these elements were normalized to their height in the spectrum of the initial (freshly quenched) sample. The performed measurements made it possible to estimate the content of lithium in the surface layer ( $\sim 0.5 \mu\text{m}$ ) and at the maximum detectable depth ( $\sim 20 \mu\text{m}$ ) of the foils, and oxygen content, in a thin surface layer (up to  $0.1 \mu\text{m}$ ). As follows from the nature of the change in the shape of the lithium signals in the spectra of instantaneous nuclear reactions with increasing annealing temperature (Fig. 4), during low-temperature annealing ( $150$  and  $220^\circ\text{C}$ ), a decrease in the lithium concentration in the analyzed surface layer is observed for  $A$  and  $B$ , including the surface region of the foils, as well as at their depth. The degree of surface oxidation increases insignificantly. With an increase in the annealing temperature, an increase in the lithium content in the detected foil layers was found. The greatest effect is observed in the spectra of instantaneous nuclear reactions of foils annealed at  $380^\circ\text{C}$ , where the lithium-signal height in the surface regions  $A$  and  $B$  increases many times. The yield of oxygen also increases in the spectra of backscattered protons.

As can be seen from Fig. 5a, the yields of  $\alpha$  particles from lithium atoms in the surface region of surfaces  $A$  and  $B$  of the initial foil and foils annealed at temperatures of  $150$ ,  $220$ ,  $300$ , and  $380^\circ\text{C}$ , are related, respectively, as  $1 : 0.86 : 0.55 : 0.80 : 2.05$  and  $1 : 0.86 : 0.55 : 0.80 : 1.48$ . At the same time, it was found that the lithium content in the array does not depend on the ana-

lyzed surface. For the initial foil and those annealed at temperatures of  $150$ ,  $220$ ,  $300$ , and  $380^\circ\text{C}$  in an array, the obtained relations were as follows:  $1 : 0.90 : 0.57 : 0.73 : 0.54$ . The layer-by-layer depth profiling of lithium in freshly quenched foils and those annealed at  $380^\circ\text{C}$  for  $1$  h, performed earlier [12] using the SIMNRA program, made it possible to construct a histogram of the change in the lithium concentration in the surface region and over the depth of the foils depending on the analyzed surface and the annealing temperature (Fig. 5b) based on the data in Fig. 5a. Thus, only for an annealing temperature of  $380^\circ\text{C}$  is the degree of enrichment of the surface region of surface  $A$   $1.4$  times higher than the surface  $B$  (Fig. 5b). In all other cases, in the studied annealing-temperature range, the lithium content near opposite surfaces of the foils is the same within the error.

In modern materials science, the concept of “melt quenching” means a heat-treatment operation associated with heating, holding and rapidly cooling a molten alloy in order to obtain materials with a unique combination of properties. Methods of centrifugal hardening, spinning, surface irradiation with electron or laser beams, as well as levitation, which make it possible to obtain high cooling rates, are used in modern experimental research and industrial technologies [10, 21]. At present, solid products pressed from rapidly solidified alloy foils are successfully used in practice, and materials for solders of corrosion-resistant coatings are being developed to strengthen composite materials. Rapidly solidified alloys are used both in the initial (foils, flakes, as well as ribbons and powders) and in the consolidated state, controlling their physical properties by heat treatment.

The rather high corrosion resistance of aluminum alloys, despite the high chemical activity of aluminum, is due to the spontaneous formation of a protective-oxide-hydroxide film on the surface of materials [22] and is explained by the phenomena of passivity in aggressive media. The corrosion resistance of alloys is

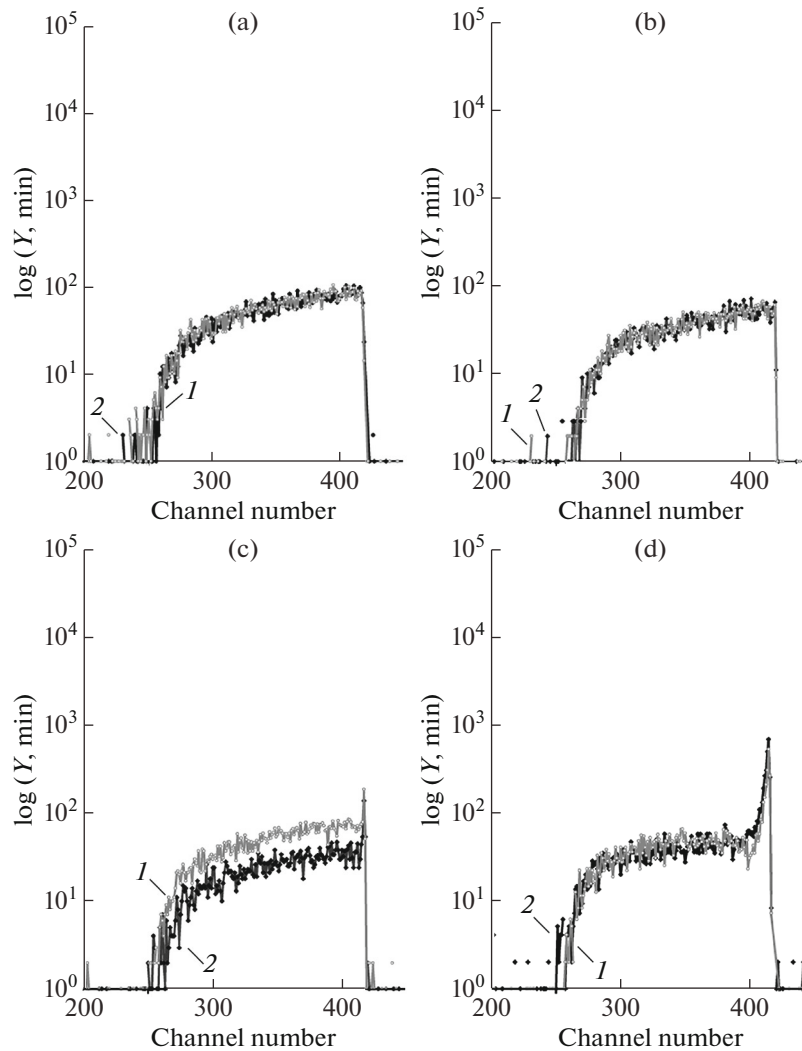


**Fig. 4.** Spectra of  $\alpha$  particles from the reaction  ${}^7\text{Li}(p, \alpha){}^4\text{He}$  for surfaces *A* (1) and *B* (2) of the 1421 alloy foils annealed at (a) 150, (b) 220, (c) 300, and (d) 380°C.

significantly affected by the structural-phase state of the surface layer, the elemental composition of which is also determined by the heat-treatment temperature. Therefore, the applied significance of the results of this study lies in the fact that the original data obtained make it possible to determine the relationship between the behavior of lithium during annealing of an alloy of the Al–Mg–Li system and phase transformations in the rapidly solidified 1421 alloy upon annealing.

Figure 6 shows a schematic diagram constructed on the basis of previously obtained results [11, 12, 23], which clearly compares the temperature dependence of the microhardness of 1421 alloy foils during isochronous annealing and the temperature intervals for the precipitation of lithium-containing phases during heat treatment. Thus, the established patterns of lithium redistribution as a result of low- and high-temperature annealing of microcrystalline rapidly solidi-

fied foils of the 1421 alloy can be explained by structural-phase changes in the samples in the studied annealing-temperature range of 150–380°C, caused by the decomposition of a supersaturated solid solution with the successive precipitation of the following intermetallic phases containing lithium: metastable  $\delta'$  phase ( $\text{Al}_3\text{Li}$ ), stable  $\delta$  phase ( $\text{AlLi}$ ), metastable phase  $S_1$  ( $\text{Al}_2\text{MgLi}$ ) and, discovered in [11], a metastable phase of variable composition  $\text{Al}(\text{Mg,Sc,Zr,Li})_x$ . The nonmonotonic nature of the change in microhardness during isochronous annealing confirms the well-known fact that the precipitation of stable phases causes the weaker hardening of alloys than the precipitation of metastable phases [24]. A significant decrease in microhardness upon heating the alloy foils above 400°C can be explained by the coarsening of intermetallic precipitates and then their dissolution, as well as recrystallization processes accompanied by

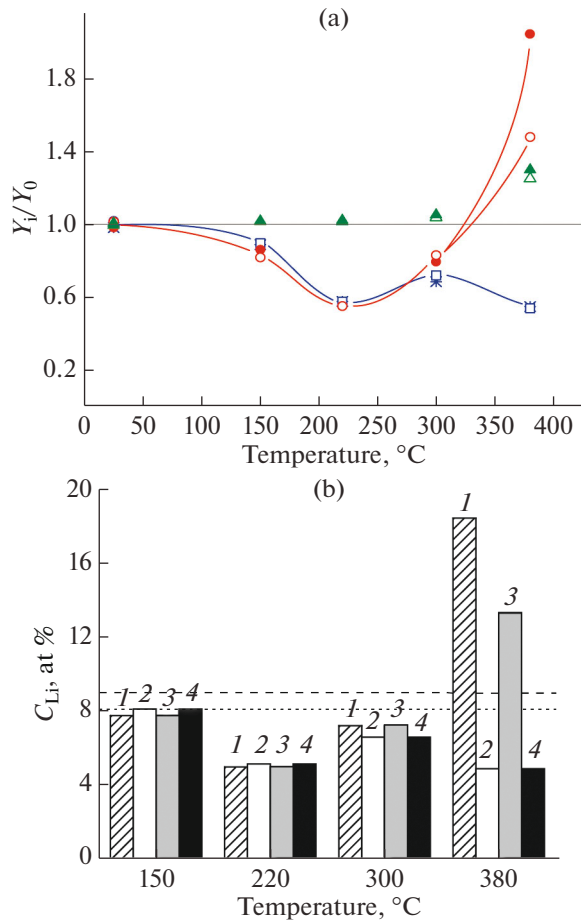


**Fig. 5.** Temperature dependence (a) of the normalized yield of lithium (circles) and oxygen (triangles) particles in the spectra of  $\alpha$  particles and protons scattered at surfaces *A* (empty symbols) and *B* (filled symbols) of foils of 1421 alloy (lithium content over depth is indicated by squares (side *A*) and asterisks (side *B*),  $Y_i$  and  $Y_0$  are the yields of the *i*th element in the experimental spectra of the annealed and freshly quenched samples, respectively). Histogram (b) of changes in the lithium concentration in the surface region (1, 3) and over the foil depth (2, 4) depending on the annealing temperature for sides *A* (1, 2) and *B* (3, 4) (horizontal dashed and dotted lines set the lithium distribution profile in the freshly quenched foil, modeled by the SIMNRA program [12], and the calculated lithium content in the 1421 alloy, respectively).

grain growth. The temperature threshold of recrystallization of the rapidly solidified alloy 1421 is increased due to the precipitation of particles of  $Al(Mg, Sc, Zr, Li)_x$  phases and  $S_1$  at the grain boundaries of the foils. This is evidenced by the results of X-ray diffraction analysis, since the texture [111], which begins to weaken at annealing temperatures above 350°C, is partially retained up to 450°C [25]. In addition, we note that using X-ray diffraction analysis it was also found that lithium reacts with oxygen on the surface of the foils, forming peroxide  $Li_2O_2$  [12].

When discussing the observed patterns of changes in the variable composition of the surface regions of an

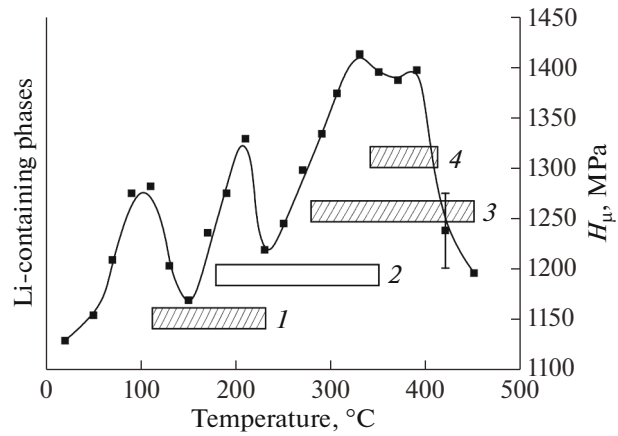


**Fig. 6.** Schematic diagram of the temperature dependence of the microhardness and phase transformations with precipitation of the lithium-containing phases  $Al_3Li$  ( $\delta'$ ) (1),  $AlLi$  ( $\delta$ ) (2),  $Al_2LiMg(S_1)$  (3),  $Al(Mg, Sc, Zr, Li)_x$  (4) in the 1421-alloy foils. The temperature intervals for the metastable phases are shown with hatching, for the stable phase, with a contour without hatching. According to our data [11, 12, 23].

alloy of the Al–Mg–Li system during heat treatment, it is necessary to pay attention to the fact that scattered and contradictory information about the behavior of lithium in aluminum alloys concerns, unfortunately, limited temperature and concentration intervals. Researchers face numerous difficulties in interpreting data obtained using indirect methods on the distribution of lithium in the surface layers of aluminum alloys [13–15, 26–28]. Rare papers report a depletion of lithium in the surface layer of the alloys as a result of annealing at elevated temperatures [14, 29–31]. On the one hand, for example, when studying passivation processes in annealed and then normalized Al–Li binary alloys, the authors of [30] report that with an increase in the calculated lithium content in the alloy from 1 to 2 wt % (from 3.4 to 7.4 at % Li, respectively), an increase in the degree of corrosion resistance is observed. The authors use the data of photoelectron spectroscopy obtained after ion etching of the surface of the alloys and explain the observed effect by the introduction of  $Li_2O$  into a passive film on the metal surface. It should be noted that in the experiment, the Al–1 wt % Li alloy was annealed at 350°C, and the Al–2 wt % Li alloy at 450°C. Unfortunately, by raising the annealing temperature, the authors did not consider the question of why the lithium concentration turned out to be 23% lower than the calculated concentration, amounting to 5.7 at % instead of 7.4 at %, on the surface of the Al–2 wt % Li alloy sample measured by photoelectron spectroscopy. In the annealed Al–1 wt % Li alloy, the measured lithium content coincided with the calculated one. In [31], the authors, reporting on the similarity of the behavior of magnesium and lithium near the surface of samples during the annealing of alloys of the Al–Mg–Li sys-

tem, related the dissolution of precipitates of the  $\delta'$  phase near the surface of the samples, which was established using transmission electron microscopy, with the formation of a surface layer depleted of lithium. Upon passing to an annealed alloy of the Al–Cu–Mg–Zn system, the authors of [31] found that the surface layer was enriched in magnesium in the absence of lithium. From this point of view, the results of the authors of [14] are of interest; they reported a tendency toward a decrease in the degree of lithium enrichment of surface layers in the annealing-temperature range of 450–570°C in the presence of such doping elements as magnesium and/or copper in comparison with Al–Li binary alloys. At the same time, after the laser-irradiation treatment of ultrafine-grained 1420 and 1421 alloys obtained by severe plastic deformation, the authors of [26, 27] report the enrichment of the oxide film with lithium, referring to the fact that lithium is an active, easily oxidizable metal. However, firstly, it should be stated that without indicating the measured numerical values of the lithium concentration, as well as the method of its depth profiling, these results can only be of a qualitative nature [26, 27]. Secondly, due to differences in the methods of obtaining samples during high-speed crystallization and severe plastic deformation, one should not expect a direct correspondence between the characteristics of the structure and physical-mechanical properties of rapidly solidified and ultrafine-grained materials.

In the present work, studies of rapidly solidified 1421-alloy foils were carried out in a relatively wide range of annealing temperatures. The established uniform distribution of lithium in the samples annealed at temperatures below 380°C indicates that a high level of concentration homogeneity of the material has been achieved due to high-speed crystallization. The main reason for the observed dependence of the lithium content in the surface layers on the heat treatment of the samples is apparently the precipitation of lithium-containing phases as a result of structural-phase transformations during annealing of the rapidly solidified alloy. For example, the redistribution of lithium in the volume of the foils in the annealing-temperature range of 150–220°C, leading to depletion of the surface and deep layers in lithium (up to 5 at % after annealing at 220°C) is apparently associated with the precipitation and then dissolution of  $\delta'$ -phase precipitates in the rapidly solidified 1421 alloy (Figs. 5b, 6), which agrees with the data of the authors of [31] described above. The subsequent precipitation of the  $\delta$  phase and the decomposition of the supersaturated solid solution with the precipitation of phase  $S_1$  are accompanied by an increase in the lithium content in the surface layers (up to 7 at %) at an annealing temperature of 300°C. Analyzing the established multiple increase in the lithium content on the surface of rapidly solidified 1421-alloy foils after high-temperature annealing at 380°C, which is accompanied by a decrease in its concentration over depth (4.9 at %), we can conclude that signif-

icant enrichment of the surface with lithium due to diffusion from the bulk to the surface of the foils is possibly associated with the dissolution of precipitates of the  $\text{Al}(\text{Mg}, \text{Sc}, \text{Zr}, \text{Li})_x$  phase, as well as structural modification of the oxide film during annealing. Therefore, in order to improve the physical and mechanical properties of alloys of the Al–Mg–Li system, including increasing their corrosion resistance, it is necessary to continue structural-phase studies in order to determine the mechanisms for the formation and evolution of the gradient structure of the surface layers of 1421-alloy foils during annealing.

## CONCLUSIONS

The obtained freshly quenched foils of rapidly solidified alloy 1421 have a microcrystalline structure and the [111] texture. The distribution of chords of random secants on grain sections by size groups can be described by a superposition of Gaussian distributions. The average grain size on the foil surface is 12  $\mu\text{m}$ . The cellular structure is observed from the side of the free surface and in the region of cavities and depressions on the contact side. The foil surface roughness varies from 44 to 57 nm.

It has been shown for the first time that the redistribution of lithium as a result of the heat treatment of foils correlates with structural-phase changes in rapidly solidified samples and is associated with decomposition of the supersaturated solid solution and the precipitation of lithium-containing phases. The dependence of the lithium content in the surface layer and over the depth of the foils on the annealing temperature has been established. In the region of low-temperature annealing, lithium is uniformly distributed over the depth of the samples within the measurement error. The lithium content in the layer being detected decreases by a factor of 1.8 in the annealing-temperature range of 150–220°C. With a subsequent increase in the annealing temperature, a gradient structure is formed in the surface layers of the foils. During high-temperature annealing (at 380°C), the surface concentration of lithium exceeds its content over depth by more than three times.

## ACKNOWLEDGMENTS

We thank leading engineer S.V. Gusakov (Interuniversity Scientific Research Service Center, Belarusian State University) for help in carrying out the experiments using the Backscattered-electron-diffraction method. I.I. Tashlykova-Bushkevich expresses gratitude to the Ministry of Education of the Republic of Belarus for the travel grant allocated for the internship at Friedrich-Schiller-Universität Jena (November 22–December 5, 2019, Jena, Germany).

## CONFLICT OF INTEREST

We declare that we have no conflicts of interest.

## REFERENCES

1. T. Dorin, A. Vahid, and J. Lamb, in *Fundamentals of Aluminium Metallurgy*, Ed. by R. N. Lumley (Woodhead, Cambridge, 2018), p. 387.  
<https://doi.org/10.1016/B978-0-08-102063-0.00011-4>
2. Y. Wang, Z. Zhang, R. Wu, J. Sun, Y. Jiao, L. Hou, J. Zhang, X. Li, and M. Zhang, *Mater. Sci. Eng., A* **745**, 411 (2019).  
<https://doi.org/10.1016/J.MSEA.2019.01.011>
3. N. I. Kolobnev, *Met. Sci. Heat Treat.* **44**, 297 (2002).
4. K. Tsakopoulos, C. Walde, V. Champagne, Jr., and D. Cote, *JOM* **71**, 435 (2019).  
<https://doi.org/10.1016/j.msea.2018.09.017>
5. V. V. Zakharov, V. I. Elagin, T. D. Rostova, and Yu. A. Filatov, *Tekhnol. Legk. Splavov*, No. **1**, 67 (2010).
6. A. V. Nokhrin, Ya. S. Shadrina, V. N. Chuvil'deev, V. I. Kopylov, A. A. Bobrov, and K. V. Likhnikitskii, *J. Surf. Invest.: X-ray, Synchrotron Neutron Tech.* **16**, 18 (2022).  
<https://doi.org/10.1134/S1027451022010116>
7. P. Dumitraschkewitz, S. A. Stephan, L. T. Stephenson, P. J. Uggowitz, and S. Pogatscher, *Adv. Eng. Mater.* **20**, 1800255 (2018).  
<https://doi.org/10.1002/adem.201800255>
8. I. Zuiko and R. Kaibyshev, *Mater. Sci. Eng., A* **737**, 401 (2018).  
<https://doi.org/10.1088/1757-899X/1014/1/012063>
9. A. L. Berezina, E. A. Segida, T. A. Monastyrskaya, and A. V. Kotko, *Metallofiz. Noveishie Tekhnol.*, No. **6**, 849 (2008).
10. W. Kurz, M. Rappaz, and R. Trivedi, *Int. Mater. Rev.* **66**, 30 (2020).  
<https://doi.org/10.1080/09506608.2020.1757894>
11. V. G. Shepelevich, I. A. Bushkevich, E. Wendler, and I. I. Tashlykova-Bushkevich, *J. Surf. Invest.: X-ray, Synchrotron Neutron Tech.* **13**, 555 (2019).  
<https://doi.org/10.1134/S1027451019030327>
12. I. A. Stoliar, V. G. Shepelevich, E. Wendler, and I. I. Tashlykova-Bushkevich, *J. Surf. Invest.: X-ray, Synchrotron Neutron Tech.* **15**, 752 (2021).  
<https://doi.org/10.1134/S1027451021040194>
13. T. Schoeberl and S. Kumar, *J. Alloy Compd.* **255**, 135 (1997).  
[https://doi.org/10.1016/S0925-8388\(96\)02818-6](https://doi.org/10.1016/S0925-8388(96)02818-6)
14. K. K. Soni, D. B. Williams, D. E. Newbury, G. Gillen, P. Chi, and D. S. Bright, *Metall. Mater. Trans. A* **24**, 2279 (1993).  
<https://doi.org/10.1007/BF02648601>
15. J.-P. Harvey, S. Singh, K. Oishi, B. Acheson, R. Turcotte, D. Pilon, J. Lavoie, and B. Gange, *Mater. Des.* **198**, 109293 (2021).  
<https://doi.org/10.1016/j.matdes.2020.109293>
16. I. S. Miroshnichenko, *Quenching from the Liquid State* (Metallurgiya, Moscow, 1982) [in Russian].
17. A. A. Suslov, V. V. Chikunov, D. I. Shasholko, and S. A. Chizhik, in *Proceedings of the VI Belarusian Workshop on Scanning Probe Microscopy BELSZM-6* (Minsk, 2004), p. 123.
18. E. Schmidt, K. Ritter, K. Gartner, and E. Wendler, *Nucl. Instrum. Methods Phys. Res., Sect. B* **409**, 126 (2017).  
<https://doi.org/10.1016/j.nimb.2017.03.111>
19. M. Mayer, *SIMNRA, A Simulation Program for the Analysis of NRA, RBS and ERDA* (Am. Inst. Phys., New York, 1999).
20. S. A. Saltykov, *Stereometric Metallography* (Metallurgiya, Moscow, 1976) [in Russian].
21. T. Pinomaa, A. Laukkanen, and N. Provatas, *MRS Bull.* **45**, 910 (2020).  
<https://doi.org/10.1557/mrs.2020.274>
22. I. V. Semenova, G. M. Florianovich, and A. V. Khoro-shilov, *Corrosion and Corrosion Protection* (Fizmatlit, Moscow, 2002) [in Russian].
23. I. A. Bushkevich, V. G. Shepelevich, I. I. Tashlykova-Bushkevich, N. V. Adintsov, M. V. Kocherga, and R. D. Lobach, in *Proceedings of the 5th International Scientific-Practical Conference Applied Problems of Optics, Computer Science, Radiophysics, and Condensed Matter Physics* (Minsk, 2019), p. 214.
24. I. I. Novikov, *Theory of Heat Treatment of Metals* (Metallurgiya, Moscow, 1986) [in Russian].
25. I. A. Bushkevich, A. V. Borodyn, Yu. E. Fishkina, and I. I. Tashlykova-Bushkevich, in *Proceedings of the VIII International Scientific Conference on Actual Problems of Solid State Physics* (Kovcheg, Minsk, 2018), Vol. **1**, p. 134.
26. P. Yu. Kikin, V. N. Perevezentsev, E. E. Rusin, and N. V. Zemlyakova, *Met. Sci. Heat. Treat.* **54**, 398 (2012).
27. P. Yu. Kikin, V. N. Perevezentsev, and E. E. Rusin, *Phys. Met. Metallogr.* **116**, 810 (2015).
28. Y. Minamino, T. Yamane, and H. Araki, *Metall. Mater. Trans. A* **18**, 1536 (1987).  
<https://doi.org/10.1007/BF02646667>
29. I. N. Fridlyander, V. S. Sandler, and T. I. Nikol'skaya, *Met. Sci. Heat. Treat.* **25**, 495 (1983).
30. H. N. Wang, C. Z. Liu, L. P. Lu, R. S. Li, and D. Lin, *Mater. Corros.* **68**, 58 (2017).  
<https://doi.org/10.1002/maco.201609083>
31. S. Fox, H. M. Flower, and D. S. McDermid, *Scr. Metall.* **20**, 71 (1986).  
[https://doi.org/10.1016/0036-9748\(86\)90215-2](https://doi.org/10.1016/0036-9748(86)90215-2)